





Electro-Thermal Behavior of Layer-Wound BSCCO Coils With and Without Insulation

A. Musso , G. Angeli , M. Ascade, M. Bocchi, P. L. Ribani , *Member, IEEE*, V. Rossi, A. Valzasina, and M. Breschi 

Abstract—In this work, the electro-thermal behavior of two layer-wound High Temperature Superconducting (HTS) coils, realized with and without electrical insulation, is compared. Both coils are wound from the same BSCCO tape, and have a very similar geometry, with the same number of turns and layers. A heat input is applied to both coils, by tuning the current supplied to resistive heaters realized through stainless steel tapes wound on the mandrel at the inner surface of both coils. The heaters are in contact with one full inner turn of the winding. The coils are cooled in a liquid nitrogen bath, and the heaters are supplied with a constant current. Then, the windings are charged until the tape critical current is exceeded, and the tests are repeated for different heat loads. The signals acquired through voltage taps, suitably soldered at the same locations in both windings, are compared at the same testing conditions. Finally, the electrical characteristic of the different layers of the coils is related to the temperature of the heater and of the various turns of the coil by means of a 1-D thermal model.

Index Terms—No-insulation coils, Superconducting coils, Layer-wound technique, Current and temperature distribution, High Temperature Superconductors.

I. INTRODUCTION

NI coils can offer a possible solution to the quench protection issues occurring in HTS devices [1]. Compared to their insulated counterpart, the current can flow also in radial direction, thus avoiding damaged/quenched areas and improving the overall thermal stability [2]–[8]. Furthermore, the heat exchange between adjacent layers is also favored by the absence of electrical insulation, which allows a more homogeneous temperature redistribution from the hot-spots [9]–[15].

In a previous work, the behavior of two layer-wound BSCCO coils of almost identical geometry, with and without insulation, was studied to compare their electrical behavior [6]. The layer-wound technique was originally selected, since not investigated extensively in the literature for NI coils [13]–[17], differently from the pancake-wound technique [18]–[26]. This work is aimed at comparing the thermal behavior of the two BSCCO

Manuscript received 29 November 2021; revised 18 March 2022; accepted 22 April 2022. Date of publication 11 May 2022; date of current version 24 May 2022. (Corresponding author: Andrea Musso.)

A. Musso, P. L. Ribani, and M. Breschi are with the Department of Electrical, Electronic and Information Engineering, University of Bologna, 40136 Bologna, Italy (e-mail: andrea.musso3@unibo.it; pierluigi.ribani@unibo.it).

G. Angeli, M. Ascade, M. Bocchi, V. Rossi, and A. Valzasina are with the RSE S.p.A., 20134 Milan, Italy (e-mail: marco.bocchi@rse-web.it).

Color versions of one or more figures in this article are available at <https://doi.org/10.1109/TASC.2022.3174512>.

Digital Object Identifier 10.1109/TASC.2022.3174512

TABLE I
TAPE AND WINDINGS PARAMETERS

HTS tape thickness [μm]	300.0
HTS tape width [mm]	4.1
Inner radius of each HTS winding [mm]	41.0
Number of HTS layers (N_L)	3
Number of HTS turns per layer (N_T)	10
Length of each layer of the NI coil [cm]	258.8 ; 260.6 ; 262.5
Length of each layer of the insulated coil [cm]	259.1 ; 261.4 ; 263.6
I_c of each layer of the NI coil (heater off) [A]	109.5 ; 109.5 ; 109.5
I_c of each layer of the insulated coil (heater off) [A]	109.5 ; 109.5 ; 113.4

coils, analyzing the electrical characteristics of the various layers in presence of a different temperature distribution inside the coils. In order to perform these analyses, a heating tape is placed in thermal contact with the entire surface of the innermost layer of the HTS tape. The setup represents a uniform heat source involving the whole coil height and propagating across the coil radial direction, as it might happen in practical cases. This also allows to adopt simplifying assumptions for the interpretative model.

Both coils are tested in a liquid nitrogen bath, by charging the HTS windings while keeping a constant current in the heater. The heater current is then varied in the test campaign in order to assess its impact on the coil electrical characteristics. The temperature distribution between the layers of the two coils is estimated using a 1-D thermal model of the coil. The model provides useful information on the impact of the interlayer insulation on the overall behavior of the coils and on the role of their respective layers.

II. EXPERIMENTAL SETUP

Two layer-wound coils are realized using a laminated *High Strength Plus* BSCCO tape manufactured by *American Superconductor Corp.* [27], cut from the same lot. The coils are wound on two G10 mandrels having an outer diameter of 80 mm. The windings have the same number of layers and turns per layer. In the NI coil, the layers are wound on top of each other without inserting any insulation. In the insulated coil, each layer is separated from the adjacent ones by a 60 μm thick Kapton layer. The main coils parameters are presented in Table I.

The manufacturing process of the coils starts with winding two layers of AISI 301 stainless steel tape in parallel (the tape is 1 cm wide and 0.3 mm thick) around each mandrel, with 6 turns per layer. The winding pitch is kept minimum, so as to form even

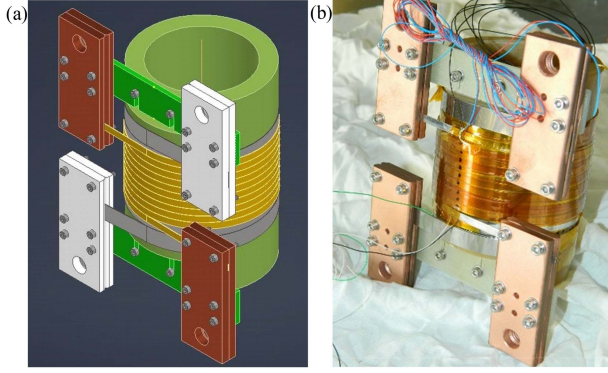


Fig. 1. Current supply connection system for the heater and the HTS coil, in (a) the CAD design phase and (b) at the end of the realization.

layers whose height over the support is greater than that of the overlying layers of the HTS winding. Then, the superconducting tape is wound around the stainless-steel layer. A 60 μm thick Kapton layer is interposed between the stainless-steel layer and the innermost HTS turn, to guarantee the electrical insulation. Finally, two layers of Kapton tape (120 μm thick in total) are wound externally to ensure the compactness of the coils. Both windings are instrumented with voltage taps soldered on the tape surface at the ends of each HTS layer.

In both coils, the HTS winding is connected to a power supply (10 V – 1.2 kA), generating current ramps of variable amplitude and duration (I_{op} is the current supplied to the HTS tape). Besides, the heater layers are connected in parallel to a different power supply system (15 V – 400 A), which injects a given current during the coil charge tests (I_h). The heater supplied current and the voltage across the voltage taps soldered at the ends of the heater are acquired during the tests. The resulting electrical resistivity is related to the temperature-resistivity characteristics $\rho(T_h)$ of the AISI 301 stainless-steel, to indirectly estimate the heater temperature, T_h . The $\rho(T_h)$ function is obtained during preliminary tests, carried out on straight segments of AISI 301 tape, supplied with a fixed current and thermally connected to a cryocooler at an initial temperature of 20 K, then slowly heated up to 300 K, so as to obtain an accurate measurement as the temperature rises.

To ensure a separate power supply between the heater layers and the HTS winding, a special design of the coil termination system is developed, whose CAD drawing is shown in Fig. 1(a), while its implementation for the NI coil is displayed in Fig. 1(b).

The tests on both coils are carried out in a liquid nitrogen bath. Before starting the power supply of the HTS tape, the heater is supplied with a constant current I_h until a thermal equilibrium is reached; I_h is maintained for the entire duration of the test. Then, the HTS windings are charged with a ramp-rate of 1 A/s, and the tests are repeated at different I_h . For each layer, the electric field is obtained as the ratio of the voltage signal across the layer and its total length, reported in Table I. Finally, the HTS supply current is shut down and the test ends when the electric field detected in any of the layers exceeds 10 $\mu\text{V}/\text{cm}$.

III. 1-D THERMAL MODEL

The experimental results are interpreted by means of a thermal model which allows one to estimate the temperature of each

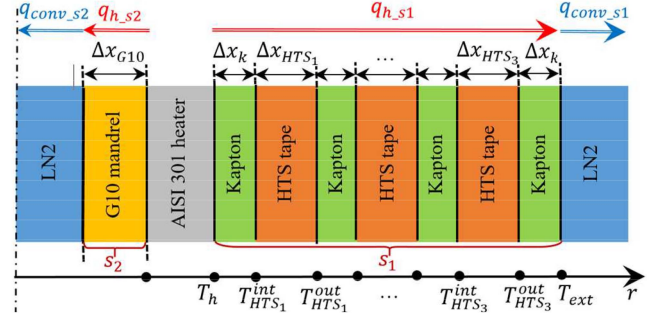


Fig. 2. Geometry and heat flows for the insulated coil, as represented in the 1-D thermal model. The figure is not in scale.

layer of the two coils. The model adopts a 1-D approximation for the winding geometry, considering heat transfer and temperature variations only in the radial direction. This is justified by assuming a cylindrical symmetry (from the thermal point of view, the layer-wound structure can be neglected for both the heater and the HTS layers) and considering the radial thickness of the whole winding as much smaller than the mandrel radius. Moreover, the calculations are performed assuming stationary thermal conditions, in which the heat input is given by the heater only. Compared to this source, the dissipation in the BSCCO tape or due to possible radial currents are considered negligible, for the type of tests performed. The heat load propagates in 2 opposite radial directions, the HTS winding (structure 1, $s1$) and the G10 mandrel (structure 2, $s2$). Fig. 2 shows how the geometry and the heat flows for the insulated coil are represented in the model. Each laminated HTS tape is represented as 3 layers stacked along the radial direction: two outer stainless-steel layers, 20 μm thick, and a central BSCCO layer.

The following heat balance equation is applied at the heater:

$$\rho(T_h) a_h j_h^2 = \sum_{i=1}^{N_{st}} f_i p_h (T_h - T_{exti}(T_h)) \left(\sum_j \frac{\Delta x_j}{k_j} \right)^{-1} \quad (1)$$

$$(T_h - T_{exti}) \left(\sum_j \frac{\Delta x_j}{k_j} \right)^{-1} = h_{conv}^{LN2} (T_{exti} - T_{LN2}) \quad (2)$$

where a_h and p_h are the cross-section and the corresponding perimeter of the heating tape. j_h is the current density supplied to the heater and N_{st} is the number of heated structures (two). f_i is the fraction of p_h in contact with the i^{th} structure, which can be eventually modified to consider different thermal contacts between layers. T_{LN2} and T_{ext} are the temperatures of liquid nitrogen and of the outermost surface of the structure, respectively. The implicit dependence of T_{exti} on T_h is presented in (2). The l.h.s. and r.h.s. of (2) represent the heat conducted through the structure (q_{h_s}) and the heat transferred to the nitrogen bath (q_{conv_s}), respectively. Δx_j and k_j are the thickness and thermal conductivity of the j^{th} layer of the structure, respectively. The heat transfer coefficient towards the nitrogen (h_{conv}^{LN2}) is a non-linear function of the temperature difference $T_{exti} - T_{LN2}$, found from a numerical fitting of the measured data. Since both the coil and the current leads are immersed in a nitrogen bath of limited size, the authors assumed the occurrence of the

film boiling regime already for low temperature differences. Moreover, the model includes temperature-dependent thermo-physical properties of the materials, obtained from MPDB [28], CRYOCOMP [29] and METALPAK [30] software. Thus, (1) has to be solved numerically to find the unknown T_h .

Since steady-state conditions are assumed to be reached, the heat transfer through the layers of each structure must be constant in time and equal to the heat flow generated by the heater. Once T_h is computed, the temperatures of all separation surfaces between the different layers can be computed in cascade using (1), starting from the layer in direct contact with the heater and moving towards the outermost layer. This leads to defining two temperatures for each layer, corresponding to its inner and outer surfaces (T_i^{int} and T_i^{ext}).

The thermal conductivity k_i is assumed constant with temperature in (1) and (2). Since the temperature of each layer is not initially known, an iterative calculation is performed starting from tentative values for the temperatures of the various layers. On subsequent iterations, k_i is computed at the mean temperature of each layer, *i.e.*, the arithmetic mean between T_i^{int} and T_i^{ext} . This procedure stops when the difference between the layer temperatures computed at subsequent iterations gets lower than a threshold tolerance.

IV. RESULTS AND DISCUSSIONS

A. Dependence of the Coil Electrical Parameters on the Heater Current and Temperature

Fig. 3 compares the electric field profiles obtained during the charging tests for the three layers of the (a) insulated and (b) NI coils (indicated as *In*, *Cen*, *Out*, for the innermost, central and outermost one). Three tests are selected for each winding, at similar T_h of both coils. It is worth noting that, at similar T_h values, the supply currents for the heaters differ substantially.

For the insulated coil, the innermost layer adjacent to the heater, reaches the critical field (*i.e.*, $1 \mu\text{V}/\text{cm}$) at lower I_{op} than the outermost layers, at the same T_h . The critical current reduction appears gradual between the three layers.

The figure does not show the curves acquired during the tests performed with $T_h = 93.7 \text{ K}$, referring to the central and outermost layers. In fact, the $10 \mu\text{V}/\text{cm}$ threshold for the current interruption is reached in the innermost layer before (or at the very beginning of) the transition of the outer layers. For these events, the critical current of the outer layers can only be obtained by extrapolating the experimental curves, extending them up to $1 \mu\text{V}/\text{cm}$ with a best-fitting procedure. These cases are shown with a dashed line, as in Fig. 3(a).

On the other hand, also for the NI coil the transition to the normal state is detected for lower I_{op} in the innermost layer compared to the other layers, during tests performed at the same T_h . However, in this case, the critical current reduction appears less gradual, as the curves corresponding to the central and outermost layers are very similar to each other. It is worth noting that the electric field measured in the central layer increases more slowly with I_{op} , compared to the other layers. This is due to a non-homogeneous current distribution between the turns of this layer, in accordance with what is described in [6]. In fact, from the models it is expected that the current flowing in

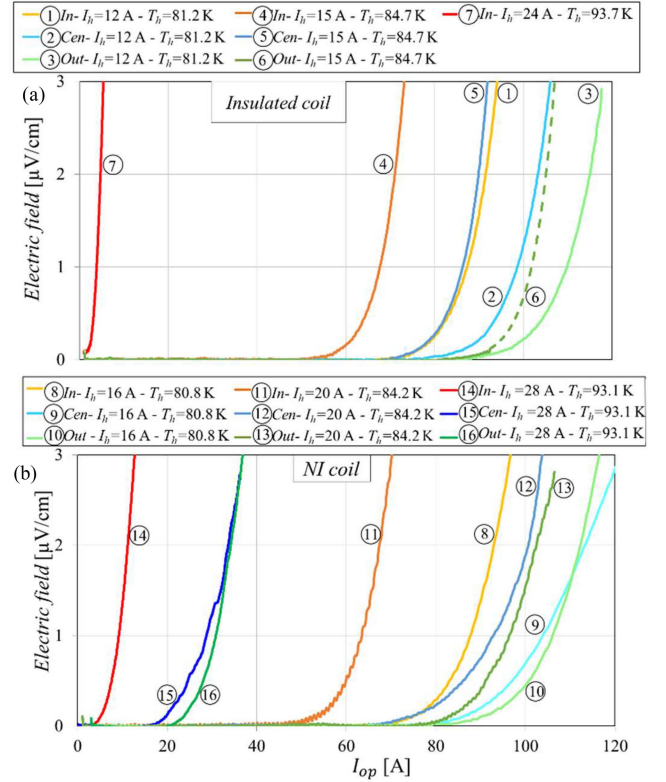


Fig. 3. Electric field profiles during charging tests carried out at different heater supply currents, for the three layers of (a) the insulated and (b) the NI coils.

some turns of the central layer is lower than I_{op} . Despite this, for the purpose of comparing the two coils, the electric fields obtained at the ends of each layer are related to the total current supplied to the superconducting winding. Similarly, the critical currents of each layer are obtained in this work as the value of the current supplied, corresponding to the critical field of $1 \mu\text{V}/\text{cm}$, regardless of the real current flowing in each turn. Thus, to avoid mis-understandings, the “effective” value of the critical current is hereafter indicated as I_c^* .

Then, Fig. 4 presents the effective critical current values measured in the different layers of the two windings (*ins.* and *NI*, in the figure), as a function of I_h , as well as those obtained for the entire coils. In both cases, I_c^* drops with increasing the heater current, and the values obtained for the whole coil are close to those measured on the inner layer, which is the most thermally stressed. In accordance with Fig. 3, for the insulated coil the I_c^* of each layer appears to decrease with decreasing the distance between the layer and the heater. For the NI coil instead, there is a considerable difference between I_c^* measured in the innermost layer and those of the central and outer layers, which are similar to each other. A similar behavior of the layers of the same NI coil, for experiments carried out with the heater turned off, has been reported in [6] and ascribed to the uneven current distribution between the layers.

In the table at the bottom of Fig. 4, some I_c^* values measured for the entire windings at similar T_h values are reported. In this case, the behavior of the two coils results similar. This implies that the presence of insulation between turns does not

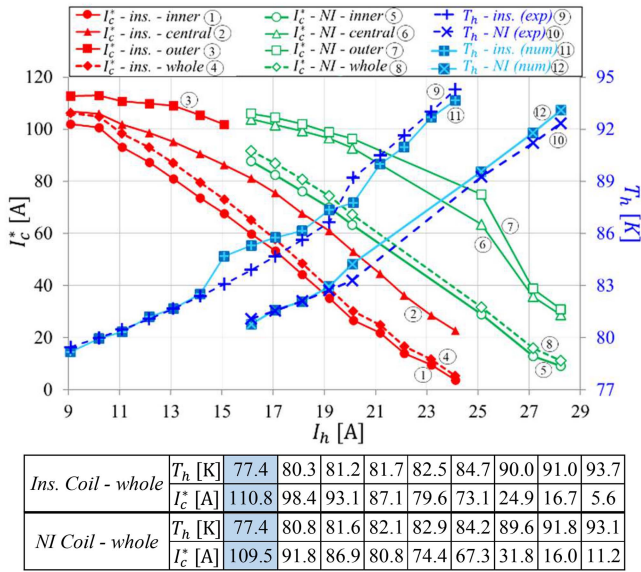


Fig. 4. I_c^* measured in the layers of the two coils for different test conditions (main axis) and numeric and experimental (I_h , T_h) curves (secondary axis). The table reports some (T_h , I_c^*) values for both windings. The highlighted cells refer to the case of heater off (data not shown in the figure).

significantly affect the electrical behavior of the winding when subjected to a heat source with the same temperature.

The dependence of T_h on the current supplied to the heater is shown in Fig. 4, with reference to the secondary axis of Fig. 4. It is worth noting that, to reach the same heater temperature, the NI coil requires greater I_h (~ 4 A higher) than the insulated one. This indicates that the absence of electrical (and thermal) insulation improves the dissipation of heat generated by the heater towards the coolant. Furthermore, a good agreement is found between the measured T_h values, obtained using the $\rho(T_h)$ function, and those computed with the model. Indeed, the thermal model provides a correct evaluation of the heat load from a heater supplied with a constant current, for both coil configurations.

B. Temperature Distribution in the Layers of the Two Coils

Fig. 5 presents the temperature distribution from the thermal model in both the insulated (5a) and NI (5b) coils. For the insulated coils, only selected cases are presented. As expected, the temperature decreases as the distance from the heater increases. The temperature drops are evident in correspondence of the insulation layers. Indeed, the HTS layers of the insulated coil operate at different temperatures, depending on their distance from the heater. This distribution explains the I_c^* trends presented in Fig. 4. Moreover, increasing the heat load, the difference between the temperatures of the different HTS layers rises.

For the NI coil, the layers present similar temperatures for the same test conditions. It has been verified that the temperature distribution is not significantly affected by the presence of facing stainless-steel laminating layers, belonging to adjacent HTS tapes. Therefore, the peculiar trend of the I_c^* curves for NI layers cannot be ascribed to the temperature distribution, but rather to the current distribution between layers, as pointed out in [6].

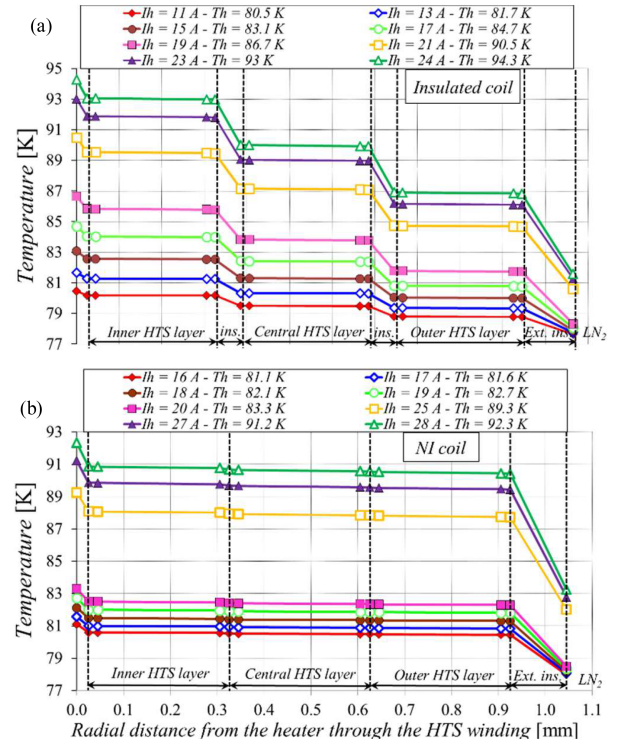


Fig. 5. Temperature distribution computed with the thermal model for (a) the insulated and (b) the NI windings, for different test conditions.

V. CONCLUSION

This paper aims at comparing the electro-thermal behavior of 2 layer-wound BSCCO coils, with and without electrical insulation. The work is relevant since the layer-wound configuration has not been extensively analyzed in the literature for NI coils, and direct comparisons of the characteristics of test coils are few. Charging tests are carried out in LN₂, to determine the effective critical current (I_c^*) of the superconducting layers. A heat load is applied to both coils, by supplying a stainless-steel tape wound around the mandrel with a constant current I_h . A 1-D thermal model is adopted to assess the temperature distribution in both windings. The heater temperatures computed with the model at different I_h agree well with those indirectly measured through the known $\rho(T_h)$ function of the heater material.

It results that, for the same heat load, the insulated coil reaches higher temperatures than the NI coil. As expected, the critical currents decrease with increasing the heater temperature. The insulation does not significantly affect the electrical characteristics of the coil when the heater temperature is the same.

In the insulated coil, the gradual I_c^* reduction approaching the heater is a consequence of the different temperatures of the HTS layers due to the electrical (and thermal) insulation.

In the NI coil, the I_c^* reduction between layers is less gradual than in the insulated one, at the same I_h . This is due to current distribution phenomena, rather than temperature gradients in the coil. In fact, the observed behaviors of the layer voltages closely resemble those measured on the same coils in absence of heater current. The same explanation given for these experimental observations, based on a non-uniform current distribution between different layers, also applies to the present case.

REFERENCES

- [1] S. Hahn *et al.*, “HTS pancake coils without turn-to-turn insulation,” *IEEE Trans. Appl. Supercond.*, vol. 21, no. 3, pp. 1592–1595, Jun. 2011.
- [2] G. Kim *et al.*, “A numerical method for spatially-distributed transient simulation to replicate nonlinear ‘defect-irrelevant’ behaviors of no-insulation HTS coil,” *Supercond. Sci. Technol.*, vol. 34, no. 11, Sep. 2021, Art. no. 115004.
- [3] S. Hahn *et al.*, “‘Defect-irrelevant’ behavior of a no-insulation pancake coil wound with REBCO tapes containing multiple defects,” *Supercond. Sci. Technol.*, vol. 29, Sep. 2016, Art. no. 105017. [Online]. Available: <https://link.springer.com/article/10.1134/S2070048215020027>
- [4] K. R. Bhattarai *et al.*, “Quench analysis of a multiwidth no-insulation 7-T 78-mm REBCO magnet,” *IEEE Trans. Appl. Supercond.*, vol. 27, no. 4, Jun. 2017, Art. no. 4603505.
- [5] M. Cho *et al.*, “Combined circuit model to simulate post-quench behaviors of no-insulation HTS coil,” *IEEE Trans. Appl. Supercond.*, vol. 29, no. 5, Aug. 2019, Art. no. 4901605.
- [6] A. Musso *et al.*, “Electrical characteristics of HTS coils with and without insulation in a layer-wound configuration,” *IEEE Trans. Appl. Supercond.*, vol. 31, no. 5, Feb. 2020, Art. no. 4900605.
- [7] A. Musso *et al.*, “Electro-thermal behavior of layer-wound BSCCO coils with and without insulation,” *IEEE Trans. Appl. Supercond.*, to be published, doi: [10.1109/TASC.2022.3174512](https://doi.org/10.1109/TASC.2022.3174512).
- [8] S. B. Kim *et al.*, “The normal-zone propagation properties of the non-insulated HTS coil in cryocooled operation,” *Phys. C*, vol. 471, pp. 1428–1431, May 2011.
- [9] D. Liu *et al.*, “Thermal stability and mechanical behavior in no-insulation high-temperature superconducting pancake coils,” *Supercond. Sci. Technol.*, vol. 31, no. 8, Jul. 2018, Art. no. 085010.
- [10] A. Ikeda *et al.*, “Transient behaviors of no-insulation REBCO pancake coil during local normal-state transition,” *IEEE Trans. Appl. Supercond.*, vol. 26, no. 4, Jun. 2016, Art. no. 4600204.
- [11] K. Katsumata *et al.*, “Influence of the turn-to-turn contact electrical resistance on the thermal stability in meter-class no-insulation REBCO pancake coils during a local normal-state transition,” *IEEE Trans. Appl. Supercond.*, vol. 27, no. 4, Jun. 2017, Art. no. 4602005.
- [12] A. Cubero *et al.*, “Electromagnetic behaviour and thermal stability of a conduction-cooled, no-insulated 2G-HTS coil at intermediate temperatures,” *Cryogenics*, vol. 108, Jun. 2020, Art. no. 103070.
- [13] S. Choi *et al.*, “A study on the no insulation winding method of the HTS coil,” *IEEE Trans. Appl. Supercond.*, vol. 22, no. 3, Jun. 2012, Art. no. 4904004.
- [14] D. Liu *et al.*, “Numerical analysis of thermal stability and mechanical response in a no-insulation high-temperature superconducting layer-wound coil,” *Supercond. Sci. Technol.*, vol. 32, Aug. 2016, Art. no. 044001.
- [15] Y. Suetomi *et al.*, “A novel winding method for a no-insulation layer-wound REBCO coil to provide a short magnetic field delay and self-protect characteristics,” *Supercond. Sci. Technol.*, vol. 32, Feb. 2019, Art. no. 045003.
- [16] Y. Suetomi *et al.*, “Mechanism of notable difference in the field delay times of no-insulation layer-wound and pancake-wound REBCO coils,” *Supercond. Sci. Technol.*, vol. 29, no. 10, Aug. 2016, Art. no. 105002.
- [17] K. Yanagisawa *et al.*, “A long charging delay for a no-insulation REBCO layer-wound coil and its influence on operation with outer LTS coils,” *IEEE Trans. Appl. Supercond.*, vol. 26, no. 6, Feb. 2019, Art. no. 4602304.
- [18] T. Oki *et al.*, “Evaluation on quench protection for no-insulation REBCO pancake coil,” *IEEE Trans. Appl. Supercond.*, vol. 26, no. 4, Jun. 2016, Art. no. 4702905. [Online]. Available: <https://aip.scitation.org/doi/full/10.1063/1.4739285?ver=pdfcov>
- [19] T. Wang *et al.*, “Analyses of transient behaviors of no-insulation REBCO pancake coils during sudden discharging and overcurrent,” *IEEE Trans. Appl. Supercond.*, vol. 25, no. 3, Jun. 2015, Art. no. 4603409.
- [20] H. Song and Y. Wang, “Simulations of nonuniform behaviors of multiple no-insulation (RE)Ba₂Cu₃O_{7-x} HTS pancake coils during charging and discharging,” *IEEE Trans. Appl. Supercond.*, vol. 26, no. 4, Jun. 2015, Art. no. 4700105.
- [21] X. Wang *et al.*, “Charging behavior in no-insulation REBCO pancake coils,” *IEEE Trans. Appl. Supercond.*, vol. 25, no. 3, Jun. 2015, Art. no. 4601805.
- [22] X. Wang *et al.*, “Turn-to-turn contact characteristics for an equivalent circuit model of no-insulation REBCO pancake coil,” *Supercond. Sci. Technol.*, vol. 26, Jan. 2013, Art. no. 035012.
- [23] S. Noguchi *et al.*, “Turn-to-turn contact resistance measurement of no-insulation REBCO pancake coils,” *IEEE Trans. Appl. Supercond.*, vol. 29, no. 5, Aug. 2019, Art. no. 4601605.
- [24] Y. Kakimoto *et al.*, “Evaluation of electromagnetic behavior of no-insulation REBCO pancake coil with multiple defects,” *IEEE Trans. Appl. Supercond.*, vol. 29, no. 5, Aug. 2019, Art. no. 4603005.
- [25] S. Hahn *et al.*, “No-Insulation coil under time-varying condition: Magnetic coupling with external coil,” *IEEE Trans. Appl. Supercond.*, vol. 23, no. 3, Jun. 2013, Art. no. 4601705.
- [26] G. Kim *et al.*, “A numerical method for spatially-distributed transient simulation to replicate nonlinear ‘defect-irrelevant’ behaviors of no-insulation HTS coil,” *Supercond. Sci. Technol.*, vol. 34, Sep. 2021, Art. no. 115004. [Online]. Available: <https://www.amscc.com>
- [27] MPDB - Material Properties Database: [Online]. Available: <https://www.jahm.com>
- [28] *Cryocomp, Rapid Cryogenic Design and Materials Properties Database - version 5.2 for Windows*, Florence, USA: Eckels Engineering, 2012.
- [29] V. Arp, *METALPAKTM, Software Version 1.10*, Littleton, USA: Horizon Technologies, Littleton, CO, Art. no. 80128.